INTERNATIONAL JOURNAL OF HYDROGEN ENERGY XXX (2017) 1–11

Available online at www.sciencedirect.com

ScienceDirect

journal homepage: www.elsevier.com/locate/he

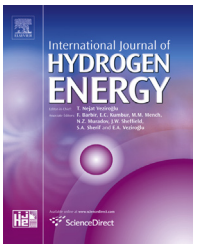

Effect of the porous stainless steel substrate shape on the ZrO_2 deposition by vacuum assisted dip-coating

*Ignacio Contardi, Laura Cornaglia, Ana M. Tarditi**

Instituto de Investigaciones en Catálisis y Petroquímica, Universidad Nacional del Litoral, CONICET, Facultad de Ingeniería Química, Santiago del Estero 2829, 3000 Santa Fe, Argentina

ARTICLE INFO

Article history:
Received 3 November 2016
Received in revised form
30 December 2016
Accepted 5 January 2017
Available online xxx

Keywords:
ZrO_2 modification
PdAu alloy membranes
Stainless steel
Tubular substrates

ABSTRACT

The effect of the support shape on the deposition of ZrO_2 by the vacuum-assisted dip-coating method was studied. Disc-shaped and tubular porous stainless steel substrates were used to obtain ZrO_2 coated supports for the synthesis of PdAu alloy composite membranes. The microstructure of the ZrO_2 modified supports was evaluated by scanning electron microscopy and confocal laser microscopy. Besides, a qualitative assessment of the porosity and roughness of the porous substrates was performed by confocal laser microscopy. Dense and continuous palladium-alloy films were deposited on top of the modified tubes after thirteen ZrO_2 deposition-calcination cycles. Cross-section EDS mapping and XRD diffraction analysis showed that a complete PdAu alloy formation was obtained even after annealing at 723 K in hydrogen stream during 5 days.

© 2017 Hydrogen Energy Publications LLC. Published by Elsevier Ltd. All rights reserved.

Introduction

Inorganic membranes have become the focus of attention during the last decades due to the possibility of their use in several industrial applications. Taking into account their almost infinite selectivity to hydrogen, palladium-based membranes are presented as an efficient material to be coupled in membrane reactors for high purity hydrogen production [1]. Furthermore, these membranes could be integrated into several industrial processes for hydrogen recovery from mixed gas streams. Despite the great advances in the development of palladium membranes, the challenge in this area is to improve mechanical stability maintaining high perm-selectivities properties.

One way to reduce cost and increase permeation flux is to use composite membranes where a thin selective layer of a palladium alloy is grown on top of a porous support. Several kinds of materials can be used as substrate for inorganic membranes, among them, the porous stainless steel is attractive due to their superior mechanical strength, and simple connection to the permeation module. Despite this, the surface pore size and roughness of the substrates difficult the deposition of a continuous, thin defect-free palladium layer on top of them. Over the last decade, several groups have considered the implementation of a modifier layer between the stainless steel supports and the palladium alloy with the attempt to avoid inter metallic-diffusion and decrease the surface pore size and roughness [2–5]. Due to

* *Corresponding author.*
E-mail address: atarditi@fiq.unl.edu.ar (A.M. Tarditi).

http://dx.doi.org/10.1016/j.ijhydene.2017.01.024

0360-3199/© 2017 Hydrogen Energy Publications LLC. Published by Elsevier Ltd. All rights reserved.

Please cite this article in press as: Contardi I, et al., Effect of the porous stainless steel substrate shape on the ZrO_2 deposition by vacuum assisted dip-coating, International Journal of Hydrogen Energy (2017), http://dx.doi.org/10.1016/j.ijhydene.2017.01.024

their thermal and chemical stabilities, zirconia and yttria-stabilized zirconia (YSZ) has been present as good materials to modify porous stainless steel supports [4,6]. PdAg and PdAu layers of a thickness between 1 and 7 μm has been deposited on top of commercially available YSZ porous stainless steel substrates by electroless plating [6,7]. Sanz et al. [8] deposited a 50 μm thick yttria-stabilized zirconia layer on porous stainless steel tubes, and used them for the synthesis of Pd composite membranes. A thickness of 27.7 μm of Pd layer was necessary to achieve a dense and defect-free membrane [8]. In a previous publication, we successfully obtained thin PdAu composite membranes on top of ZrO_2-modified porous stainless steel discs [9]. The modification of the support was performed by means of the vacuum-assisted dip-coating method using a commercial colloidal suspension as a source of ZrO_2. In addition of allowing the decrease of the Pd layer thickness, the ZrO_2 coating between the stainless steel and the Pd-based alloy, effectively avoids the inter-metallic diffusion within their components. In our samples, no composition gradient was detected on thickness after permeation experiments as determined by cross-sectional EDS line scan [9]. Lin and coworkers [10] reported a significant improve in the thermal stability using YSZ as intermediate layer between palladium and porous stainless steel discs substrates at temperatures above 873 K [10]. On the other hand, Okazaki et al. [11] have shown constant hydrogen permeation and selectivities for palladium membranes supported on YSZ-porous supports instead of alumina, at temperature as higher as 923 K [11]. From SEM and XPS experiments, migration of yttria or zirconium was not observed onto the palladium layer [11].

Palladium alloy membranes could be growth on top of porous substrates by mean of several deposition techniques as well as chemical vapor deposition, physical vapor deposition, electroplating and electroless plating [12]. Among them, the electroless deposition techniques have received much attention considering their advantages, namely applicability on substrates of different shapes, low cost and simplicity [12,13]. Although the electroless deposition of composite palladium membranes could be performed on top of planar and tubular substrates, tubular membranes are the more suitable option to be applied at industrial scale. Even though planar membranes are simple to prepare and well-suited with a range of seal designs, they have a low surface area and a large sealing/membrane area ratio. On the other hand, tubular membranes exhibit a higher surface area to volume ratio and they present the advantage of an easier assembly to the permeation module [14].

The main objective of the present study was to optimize the deposition of a ZrO_2 layer on the outer surface of porous stainless steel tubes and analyze the influence of the substrate shape (disc or tube) on the ZrO_2-modification by the vacuum-assisted dip-coating method. The microstructure of the samples after several deposition-calcination cycles was analyzed by scanning electron microscopy (SEM) and confocal laser microscopy (FCOM). PdAu layers were synthesized by the electroless deposition technique on top of the ZrO_2 modified porous stainless steel tubes. The permeation properties of the membranes were studied as a function of temperature and pressure.

Experimental

Membrane preparation

ZrO_2 modification of tubular supports

For the synthesis of the composite membranes, porous stainless steel tubes 0.2 μm grade (Mott Metallurgical Corporation) were used as substrates. The tubes were cleaned and oxidized following the procedure previously reported [15]. With the attempt to avoid inter-metallic diffusion and reduce surface pore size, the outer surface of the tubes were modify with zirconium by the dip-coating method using a commercial ZrO_2 suspension (Nyacol Acetate Stabilized 20 wt.%, particle size between 5 and 10 nm) [9]. The supports were subjected to sequential deposition-calcination cycles; each cycle consisted of three ZrO_2 dip-coatings; afterward, the support was dried at room temperature for 1 h and the following dipping was performed. Finally, it was calcined at 673 K for 3 h. The vaccum-assisted deposition method was used in the last deposition cycles. Additional details regarding modifications are presented on our previously publication [9]. The number of ZrO_2 deposition cycles on the tubular supports was optimized in order to improve the pore-filling. Fig. 1 shows a scheme of the setup used for the ZrO_2 deposition on disc shaped and tubular substrates. For a comparison a porous disc was modified with five deposition-calcination cycles under the same conditions than those reported elsewhere [9].

PdAu layers deposition

The sequentially electroless plating method was used to synthesized the PdAu alloy film on the outer surface of the tubular supports. Before to the metallic deposition, the modified supports were activated using the conventionally sensitization-activation stage described elsewhere [9]. After that, the palladium and gold layers were deposited using the bath compositions reported previously [9]. First, palladium was deposited in two steps for 60 min each at 323 K, followed

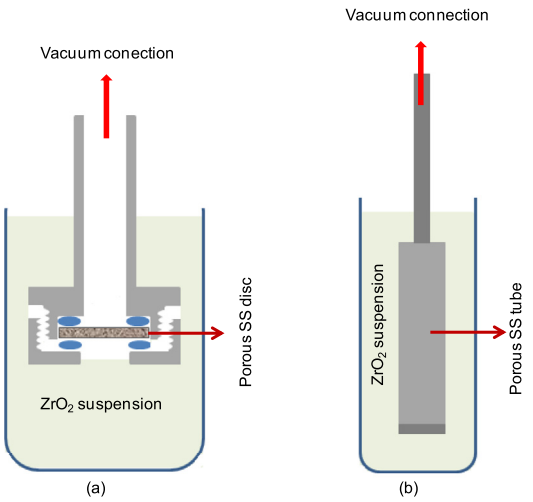

Fig. 1 – Schematic diagram of the vacuum-assisted dip-coating method for disc shaped (a) and tubular (b) supports.

Please cite this article in press as: Contardi I, et al., Effect of the porous stainless steel substrate shape on the ZrO_2 deposition by vacuum assisted dip-coating, International Journal of Hydrogen Energy (2017), http://dx.doi.org/10.1016/j.ijhydene.2017.01.024

by an gold deposition of 20 min at 333 K. After the Pd and Au depositions, the samples were rinsed with water and dried at 393 K overnight. The synthesis procedure was repeated until the composite membrane became impermeable to N_2 at room temperature and at a pressure difference of 10 kPa. Then, the samples were heated up to 723 K or 773 K in a hydrogen atmosphere to promote the metallic inter-diffusion and alloy formation. The temperature of the reactor was increased from room temperature up to the annealing temperature with a heating rate of 0.5 K min^{-1} in nitrogen flow and then, the annealing process was conducted in hydrogen atmosphere. The final film thickness was estimated from the weight gain and checked by SEM.

The nomenclature used for the modified supports was ZrO_2-XZ, where X refers to the number of deposition-calcination cycles and Z the support shape, D and T for disc and tube, respectively. The main characteristics of the synthesized samples are summarized on Table 1.

Table 1 – Main characteristics of the samples studied.

Sample	Shape	Cycles[a]	PdAu thickness (μm)
ZrO_2-5D	Disc	5	–
ZrO_2-5T	Tube	5	–
ZrO_2-10T	Tube	10	–
ZrO_2-13T	Tube	13	–
PdAu–ZrO_2-5D	Disc	5	12
PdAu–ZrO_2-5T	Tube	5	33
PdAu–ZrO_2-10T	Tube	10	27
PdAu–ZrO_2-13T	Tube	13	13

[a] ZrO_2 deposition cycles: each cycle consists of three ZrO_2 coatings followed by drying at RT 12 h and calcination at 673 K for 3 h.

Sample characterization and permeation measurements

X-ray diffraction measurements before and after annealing were performed with an XD-D1 Shimadzu instrument, using Cu Kα (λ = 1.542 Å) radiation operating at 30 kV and 40 mA. The scan rate was 1°min^{-1} in the 2θ = 15–90° range.

The top surface and cross-sectional images of the samples were characterized by Scanning Electron Microscopy (SEM) using a JEOL (JSM-35C) microscope. An energy dispersive analytical system (EDAX) coupled in the microscope were used to determine the bulk atomic composition of the ZrO_2 modified supports and the PdAu layers after annealing. The cross-section EDS-mapping of the PdAu membranes was obtained using a Zeiss FEG-SEM instrument, model SUPRA 40, equipped with an energy dispersive analytical system (Oxford Instruments).

The measurements of the surface and line profile roughness of the samples were performed using an Olympus LEXT 3D OLS4000 confocal microscope (405 nm laser excitation). The scanning mode XYZ step was used with an image size of 258 × 258 μm. The images were analyzed using the LEXT software.

Hydrogen and nitrogen single gas permeation measurements were performed using a tubular permeation module reported elsewhere [16]. The permeator was placed in an electric furnace and heated up to the desired temperatures at heating rate of 0.5 °C/min.; the temperature was controlled with a thermocouple placed in the membrane size. The Pd alloy side of the membrane was flushed with feed gases, while the other side was flushed with N_2 as sweep gas (permeate side) during the heat procedure. No sweep gas was used on the permeate side during the single-gas permeation experiments. All the gases were fed to the permeator using calibrated mass-

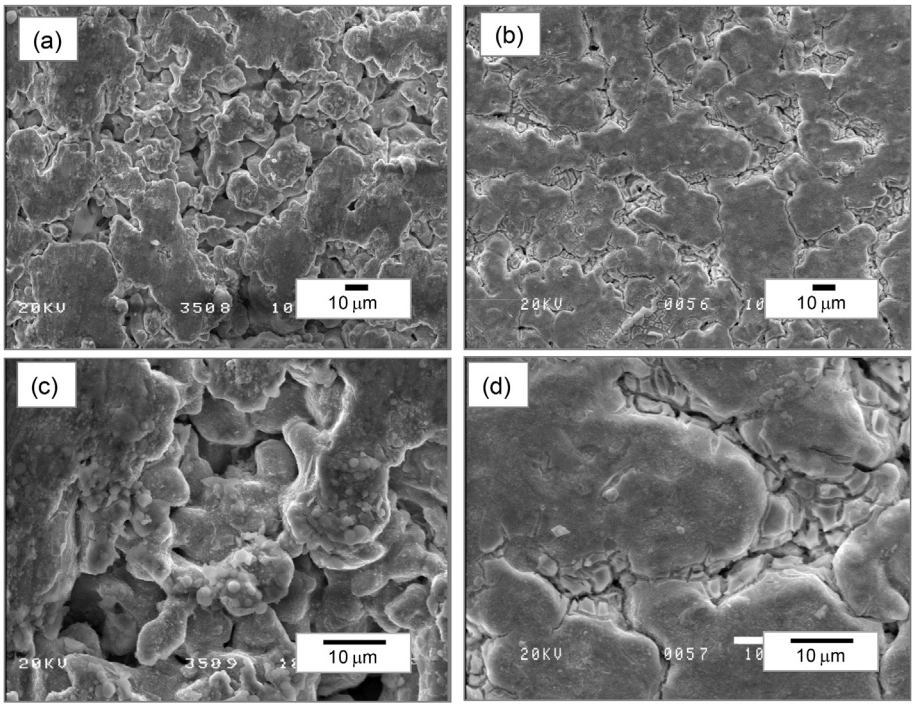

Fig. 2 – Tubular (a, c) and disc shaped (b, d) porous stainless steel supports modified by ZrO_2 with five deposition-calcination cycles.

Please cite this article in press as: Contardi I, et al., Effect of the porous stainless steel substrate shape on the ZrO_2 deposition by vacuum assisted dip-coating, International Journal of Hydrogen Energy (2017), http://dx.doi.org/10.1016/j.ijhydene.2017.01.024

flow controllers and pressure differences across the membranes were controlled using a back-pressure regulator. The upstream was varied while keeping the downstream pressure constant at 100 kPa. Bubble flow meters were used to measure the hydrogen or nitrogen permeation flow rates. The permeation areas of the tubular membranes were ca. 4.2 cm^2. The flux measurements were performed at temperatures between 673 and 723 K and ΔP between 10 and 100 kPa. All temperature changes were carried out in N_2 atmosphere.

Results and discussion

Optimization of the ZrO_2 deposition on stainless steel tubular supports

It has been shown that the ZrO_2 modification of porous stainless steel discs by the vacuum-assisted dip-coating method enables the formation of defect-free PdAu composite membranes of ca. 10 μm thickness, with improved thermal stability [9]. Taking into account that tubular membranes are more suitable from a practical point of view, the optimization of the ZrO_2 modification on the outer surface of tubular porous stainless steel was studied in the present work.

Fig. 2 shows the SEM surface top view of a tubular (ZrO_2-5T) and planar (ZrO_2-5D) porous stainless steel support (0.2 μm grade) after five deposition-calcination cycles. It can be observed that, after five deposition-calcination cycles, the pores filling in the tubular support is not as high as the coverage observed in the planar support. In a previous publication, we reported that for both 0.1 and 0.2 μm flat supports, a complete coverage of the porous surface and a smoother surface were observed after five deposition-calcination cycles (Fig. 2b and d) [9]. Contrary to these findings, when the same number of deposition-calcination cycles was performed on the outer surface of tubular substrates, a complete pore-filling and a heterogeneous coverage of the support were not observed (Fig. 2a and c). This could be due to the fact that, compared with the morphology of the unmodified discs (Fig. 3), the tubular substrate has a more heterogeneous pore distribution and perpendicular growth of stainless steel grains with a rougher surface (Fig. 3a). Comparing the top surface morphology of the planar (Fig. 3b) and tubular (Fig. 3a) supports, it is possible to note that the tubes present a large pore volume and open structure at the surface (Fig. 3). Additionally, when the cross-section images of the disc (Fig. 3d) and tube (Fig. 3c) are compared, it is possible to observe a more porous open structure in the tubular shape. Although both shapes (planar and tubular) have the same pore grade (0.2 μm) as reported by the manufacturer, they present a different surface roughness and topography, probably due to the different manufacturing methods.

In order to perform a deeper comparison of the roughness properties between the two shapes, 0.2 micron grade tube and disc supports were analyzed by confocal laser microscopy. Fig. 4 shows the confocal images obtained for the tubular and planar supports and the line profile analysis. Note that for the tubular support, a higher peak to valley depth of about 24–27 μm is observed in the profile (Fig. 4a), while on the planar support the maximum depth is ~14 μm (Fig. 4b). Table 2 shows the maximum peak height (*Pp*), maximum valley height (*Pv*) and maximum height of primary profile (*Pt*) parameters obtained from the line roughness analysis.

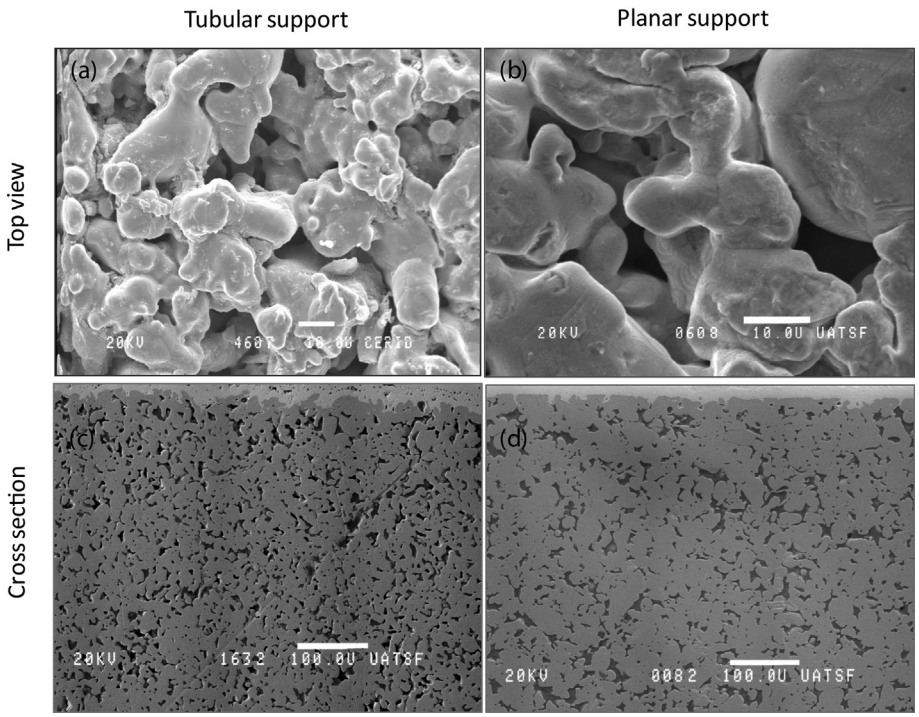

Fig. 3 – Microstructural comparison between tubular and disc shaped supports. SEM images for surface top-view of: (a) tubular support, (b) disc shaped. Cross-section: (c) for tube and (d) for disc.

Please cite this article in press as: Contardi I, et al., Effect of the porous stainless steel substrate shape on the ZrO_2 deposition by vacuum assisted dip-coating, International Journal of Hydrogen Energy (2017), http://dx.doi.org/10.1016/j.ijhydene.2017.01.024

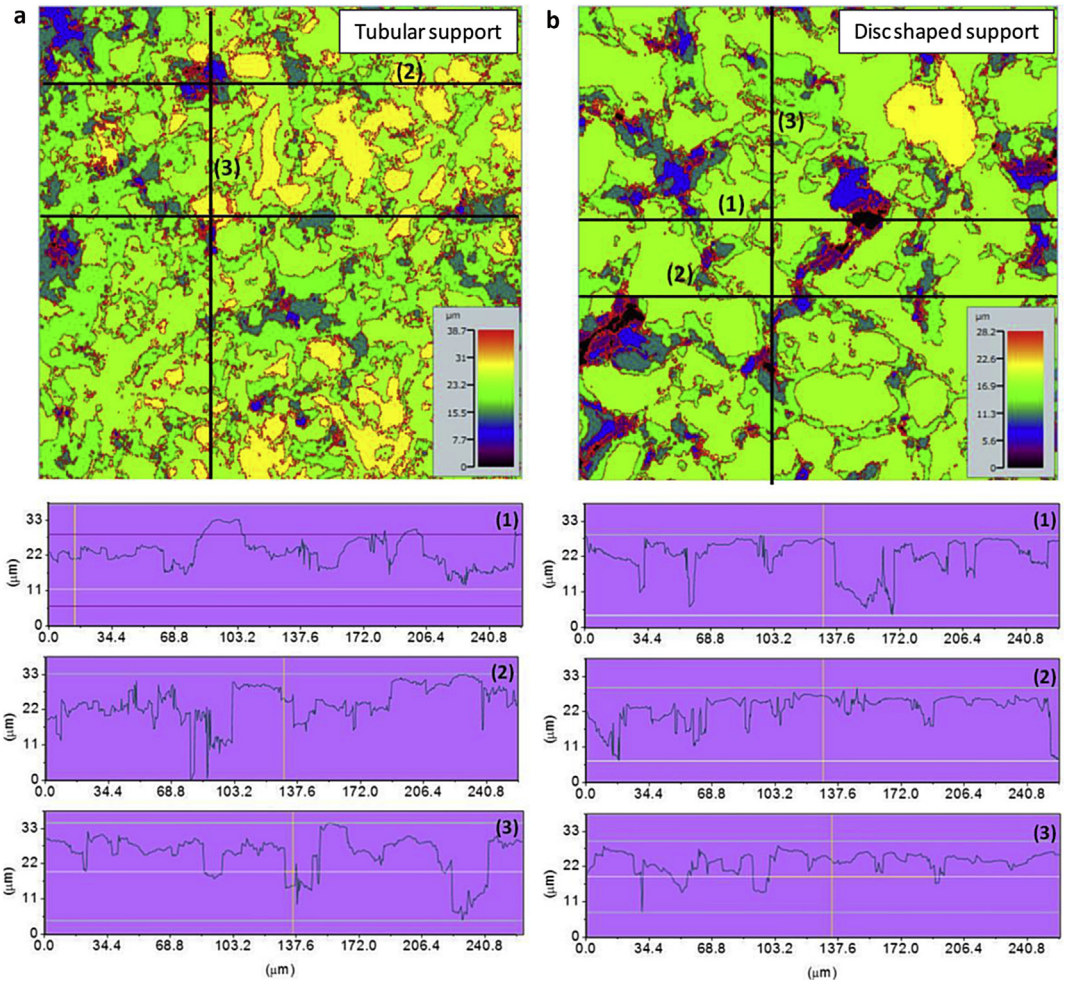

Fig. 4 – Confocal laser images and line profile analysis of the tubular (a) and disc shaped (b) supports.

Based upon the observations on the ZrO_2-5T sample, five additional dipping, drying and calcination cycles were performed in a tube, (ZrO_2-10T sample) in order to increase the pore-filling. Fig. 5 shows the SEM top surface view corresponding to two different zones (a, b zone 1 and c, d zone 2) of the support after ten deposition-calcination cycles at two magnifications. A homogeneous distribution of ZrO_2 on the porous substrate can be observed from the images taken in the two regions of the surface (Fig. 5). Note that a higher coverage of the porous was obtained compare with the sample with five deposition-calcination cycles; however, the coverage was not as high as that obtained on top of the disc with five deposition cycles (ZrO_2-5D sample) (Fig. 2d).

Fig. 6a shown the surface morphology of the ZrO_2-13T sample after thirteen deposition-calcination cycles. It was observed that the ZrO_2 coverage was improved (ZrO_2-13T sample), yielding an uniform and almost complete coverage of the porous surface (Fig. 6b). From the cross-section obtained by SEM-EDS, a thin layer of ZrO_2 was observed in this sample (Fig. 6c). After the ZrO_2 modification, the average peak to valley depth determined by confocal microscopy decreases from 22.3 μm for the unmodified tube up to 10.9 μm and 8.2 μm for the ZrO_2-10T and ZrO_2-13T samples, respectively (Table 2). This indicates that the pore depth in the modified support is on average lower than those in the unmodified support, consistent with the top-view SEM observations (Figs. 5 and 6).

It has been reported that for the deposition of a ceramic layer by dip-coating on a porous support, the following properties are of primary importance: pore size and size distribution, porosity, roughness, surface and bulk homogeneity. Then, one of the critical parameters governing the formation of the initial layer on a dip-coating process is the ratio between the particle diameter in the suspension and the pore size of the support [17]. This statement is in agreement with our observation that in the planar supports, with a lower pore size at the surface, it was easier to obtain a complete coverage of the pores with lower number of deposition cycles. Note that the pore size on the surface of the unmodified tubular support has a wide distribution ranging from 10 to 30 μm with some larger pores of up to 40 μm (Fig. 3). On the other hand, the pore size on the surface of the planar support is between 10 and 20 μm (Fig. 3). The morphological analysis shows that the pore diameter at the surface of the tubes is larger than those of discs for substrates with the same grade reported by the manufacturer. Using mercury intrusion measurements, Mardilovich et al. [18] reported a bulk pore size distribution

Please cite this article in press as: Contardi I, et al., Effect of the porous stainless steel substrate shape on the ZrO_2 deposition by vacuum assisted dip-coating, International Journal of Hydrogen Energy (2017), http://dx.doi.org/10.1016/j.ijhydene.2017.01.024

Table 2 – Some analysis parameters in the line roughness analysis performed with confocal laser microscopy.

Sample	*Pp* (Max.) (μm)	*Pp* (average) (μm)	*Pv* (Max.) (μm)	*Pv* (average) (μm)	*Pt* (Max.) (μm)	*Pt* (average) (μm)
Tube (0.2 μm)	15.8	8.1	21.9	14.8	34.5	22.9
Disc (0.2 μm)	8.2	4.5	16.4	10.2	23.7	14.8
ZrO_2-10T	5.6	4.2	9.1	6.6	14.5	10.9
ZrO_2-13T	3.8	3.5	7.8	5.3	11.5	8.8

Pp: Maximum peak height; *Pv*: Maximum valley height; *Pt*: maximum primary height of primary profile (the sum of *Pp* and *Pv*).

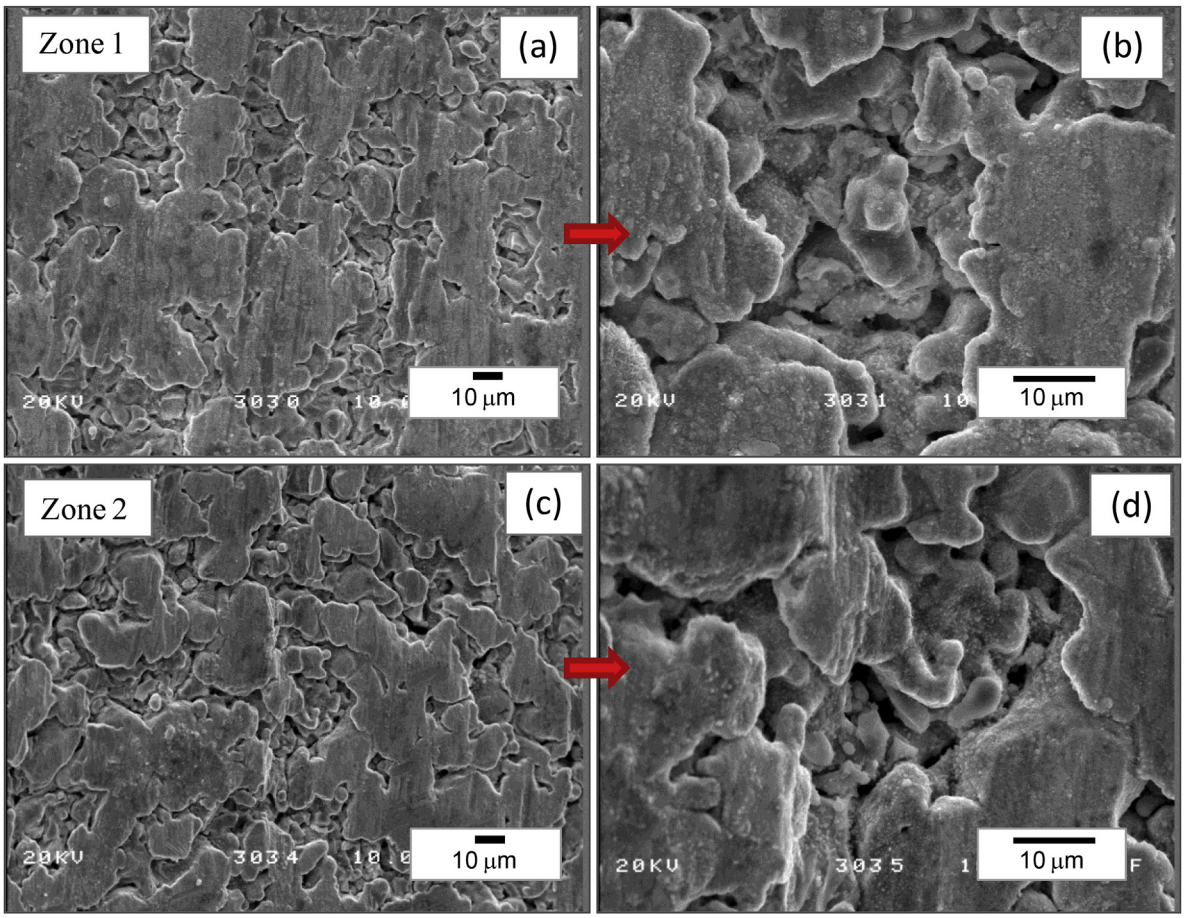

Fig. 5 – SEM images for tubular support modified with 10 deposition-calcination cycles (ZrO_2-10T sample) in two different zones: (a, b) zone 1 and (c, d) zone 2.

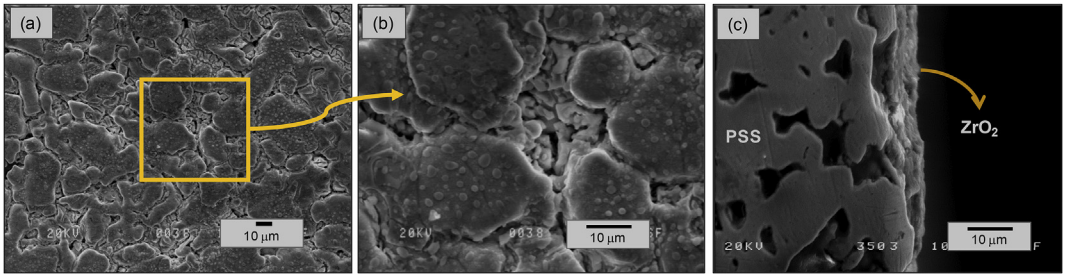

Fig. 6 – SEM top view (a, b) and cross-section (c) of a tubular support modified with 13 cycles of ZrO_2 (ZrO_2-13T sample).

Please cite this article in press as: Contardi I, et al., Effect of the porous stainless steel substrate shape on the ZrO_2 deposition by vacuum assisted dip-coating, International Journal of Hydrogen Energy (2017), http://dx.doi.org/10.1016/j.ijhydene.2017.01.024

ranging between 0.6 and 7 μm for a porous stainless steel tube of 0.2 μm grade, with a larger pore size at the surface. An average pore size of ca. 2.25 μm and a distribution in the range of 0.75–3.25 μm for similar supports have been determined by the bubble-point pressure method [19]. The data suggest that the pore entrance at the surface is larger than those in the bulk of the support.

By mean of the vacuum assisted dip-coating method and optimizing the number of deposition-calcination cycles, we could obtained a smooth and homogeneous ZrO_2 coating on top of porous tubular supports. In comparison with other modification techniques reported in the literature for deposition of ZrO_2 or YSZ such as magnetron sputtering [20] or atmospheric plasma spraying [8,21] this is a simpler and cheaper method which could be easily scalable. Fernandez and coworkers [8] have deposited a thick (ca. 50 μm) YSZ layer on stainless steel porous tube by atmospheric plasma spraying. The improvement with respect to our previously work [9] was the optimization of ZrO_2 deposition on tubular instead of disc substrates. From the data reported here it is possible to conclude that the support shape (disc or tube) has a significantly influence on the features of ZrO_2 coating.

Properties of the PdAu layers synthesized on top of the ZrO_2 modified porous stainless steel tubes

With the aim to be applied as membranes for hydrogen purification, PdAu layers were deposited by the sequential electroless deposition technique on top of the ZrO_2 modified tubular supports. The effect of the ZrO_2 coverage on the thickness and morphology of the PdAu layers was analyzed by SEM-EDS.

Fig. 7 shows the top surface images of the samples synthesized on the outer surface of porous stainless steel tubes after 5 (a, d), 10 (b, e) and 13 (c, f), ZrO_2 deposition-calcination cycles. As it can be observed in the figure, the surface of the tubular PdAu–ZrO_2-5T sample (Fig. 7a and d) was not covered by a continuous PdAu alloy layer even after ten electroless deposition cycles (one cycle: two Pd plating of 60 min each followed by a Au plating of 20 min). Note that a rougher surface made up of irregular clusters with high defect density was obtained under these conditions (Fig. 7d). From the weight gain measurements, a thickness of about 33 μm was estimated for this sample. On the other hand, the PdAu–ZrO_2-10T membrane (Fig. 7b and e) presented an improvement in the coverage of the support with smaller clusters and defect density after seven deposition cycles (ca. 25 μm from weight gain). For this membrane, no nitrogen permeation was observed after drying at 393 K at room temperature. However, after annealing at 773 K the membrane presented a loss of selectivity, reaching a H_2/N_2 ideal selectivity of 215 at 673 K and 100 kPa, which could be due to presence of defects on the surface of the PdAu layer (Fig. 6). The membrane synthesized on top of the porous support modified with thirteen ZrO_2 deposition-calcination cycles (PdAu–ZrO_2-13T membrane) presented a smoother surface with a compact PdAu layer on top of the modified support (Fig. 7c, f), with no evidence of defects. This membrane did not present nitrogen permeation even after annealing up to 723 K under hydrogen stream.

It is known that the thickness and quality of the Pd alloy layer deposited on top of a porous substrate depends on both the deposition method and the support properties such as pore size distribution and defect density. For achieving a dense palladium layer by electroless deposition, a minimum thickness of approximately three times the diameter of the largest pores in the supports was needed, as reported by Mardilovich et al. [18].

The PdAu–ZrO_2-13T membrane was annealed at a lower temperature with the aim to optimize the PdAu alloy formation at a lower temperature. From the XRD analysis of both the PdAu–ZrO_2-10T and PdAu–ZrO_2-13T membranes, a complete alloy formation was observed after annealing up to 773 and 723 K, respectively, during 162 h (Fig. 8).

Fig. 9 shows the cross-section view of the PdAu–ZrO_2-10T and PdAu–ZrO_2-13T membranes. The PdAu–ZrO_2-13T membrane (Fig. 9a) exhibits a lower thickness (mean

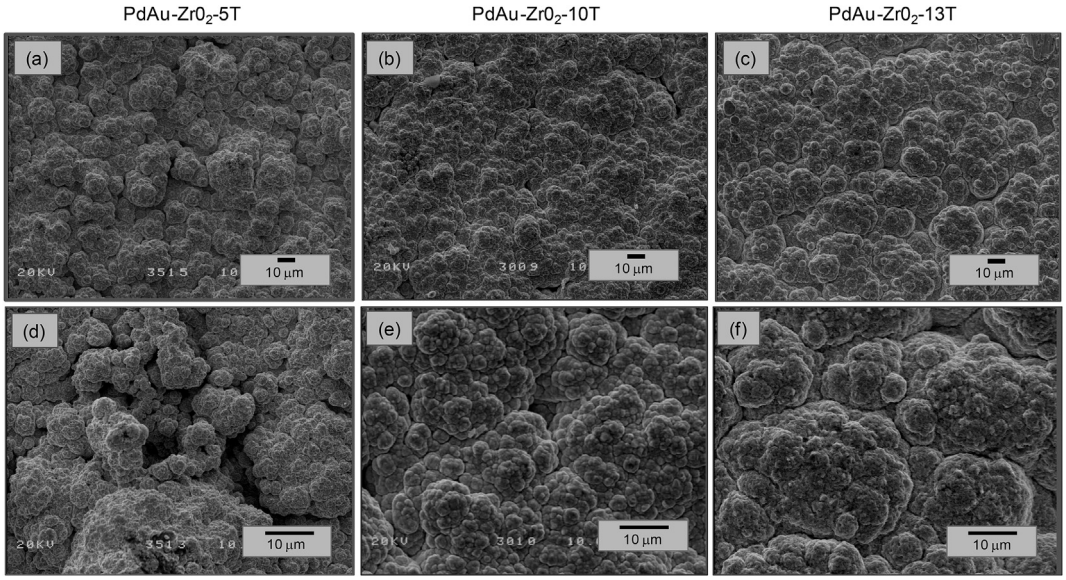

Fig. 7 – SEM top surface view of the PdAu membranes synthesized on top of ZrO_2 tubular modified supports.

Please cite this article in press as: Contardi I, et al., Effect of the porous stainless steel substrate shape on the ZrO_2 deposition by vacuum assisted dip-coating, International Journal of Hydrogen Energy (2017), http://dx.doi.org/10.1016/j.ijhydene.2017.01.024

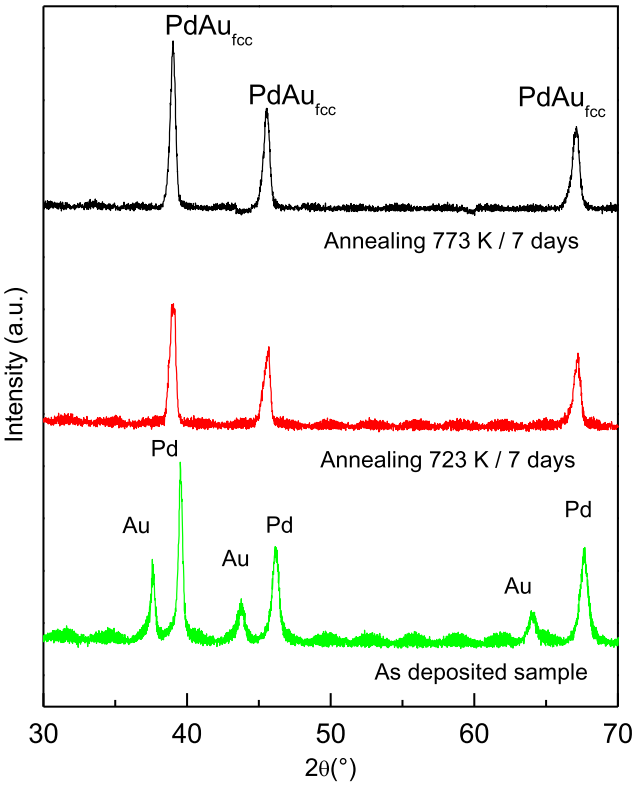

Fig. 8 – XRD diffraction patterns of a PdAu as deposited sample, after annealing at 723 K and 773 K for seven days.

thickness = 14 μm) in comparison with the thickness of the PdAu–ZrO_2-10T membrane (Fig. 9b, mean thickness = 27 μm). The SEM-EDS measurements show a homogeneous Pd and Au distribution on thickness with no evidence of diffusion of components of the stainless steel substrate for both membranes. Note that the PdAu layers of both membranes are dense with low defect density and they are well adhered to the support. The Pd, Au and Fe X-ray compositional mapping is shown in Fig. 10. It is possible to see a homogeneous distribution of Pd and Au in the alloy layer with no diffusion of Fe from the support. Zr was not detected in the X-Ray mapping analysis; however, when EDS local spot scans were performed in the PdAu-support interface, Zr was detected in a low amount. These data are in agreement with the XRD data in which a complete alloy formation was observed even after 723 K (Fig. 8). The PdAu alloy formation from the electroless plating of sequential palladium and gold thin layers on top of ceramic tubes was studied by Goldbach and coworkers [22]. The analysis of the alloy formation as a function of time at different temperatures showed that the alloying of the Pd and Au separate metal layer required about 168 h at 873 K and more than 500 h at 773 K under hydrogen stream. When the PdAu membranes were prepared from the electroless deposition of alternated palladium and gold nano-structured layers, the authors reported complete alloy formation at 773 K [23]. The multilayer pattern observed by SEM-EDS in the as-deposited film disappeared and the Pd and Au EDS traces became flat after one day of annealing at 773 K under atmospheric hydrogen pressure, which indicated that the homogenization of the multilayer proceeded rapidly under those circumstances [23]. The improved alloying of nano-structured PdAu electroless deposited films could be attributed to the much extended interface between the two metals in comparison with a bilayer film with the same total thickness. In the same line, we found a complete PdAu fcc alloy formation at 773 K during 120 h in hydrogen stream and 10 kPa of difference of pressure through the membrane, for multilayered Pd/Au films synthesized on top of porous stainless steel discs [9]. In the membranes studied in the present work, a homogeneous alloy formation on thickness was obtained even after annealing at 723 K during 168 h, as it can be seen from the EDS-mapping shown in Fig. 10.

The permeation properties of the as synthesized PdAu membranes were evaluated as a function of temperature and pressure drop between the retentate and permeate side of the membrane. Fig. 11 shows the hydrogen permeation flux at 673 K for the PdAu–ZrO_2-10T and PdAu–ZrO_2-13T membranes as a function of pressure differences between 10 and 100 kPa; the data were obtained after annealing in hydrogen stream during 5 days. Note that the hydrogen flux through the

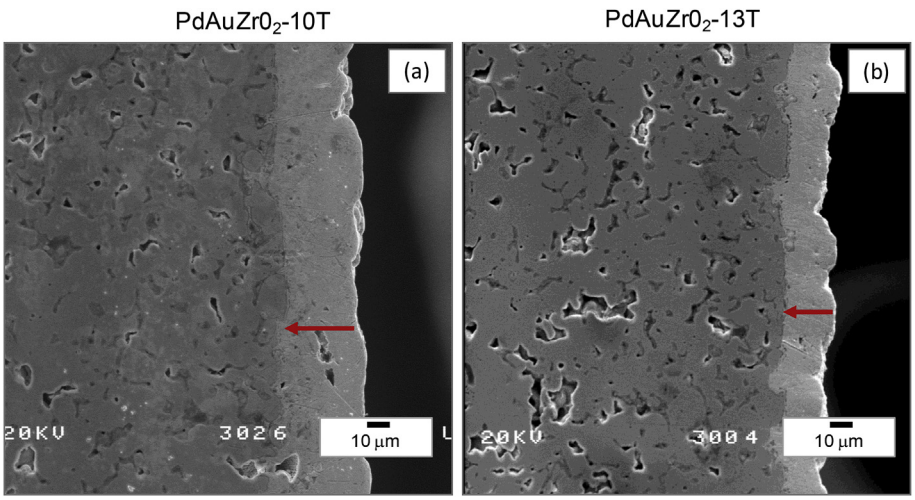

Fig. 9 – SEM cross-section view of the membranes PdAu–ZrO_2-10T (a) and PdAu–ZrO_2-13T (b) membranes.

Please cite this article in press as: Contardi I, et al., Effect of the porous stainless steel substrate shape on the ZrO_2 deposition by vacuum assisted dip-coating, International Journal of Hydrogen Energy (2017), http://dx.doi.org/10.1016/j.ijhydene.2017.01.024

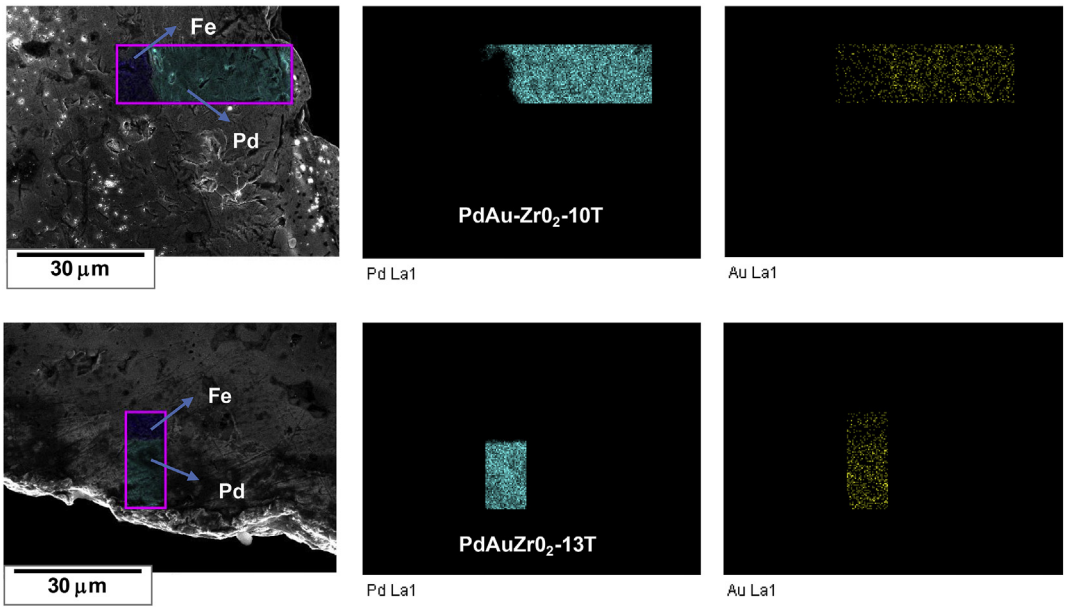

Fig. 10 – X-ray mapping in the SEM cross-section images of the PdAu–ZrO_2-10T (top) and PdAu–ZrO_2-13T (bottom) membranes.

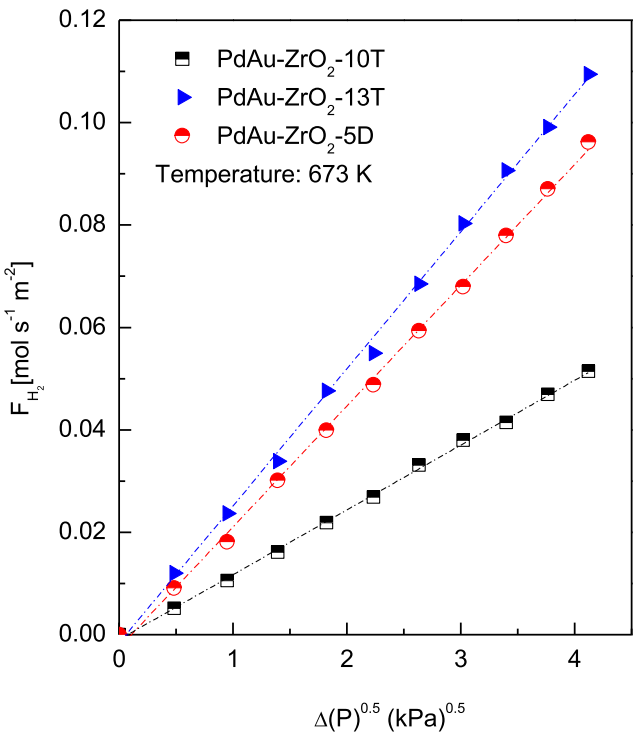

Fig. 11 – Hydrogen permeation flux of the PdAu membranes as a function of $\Delta(P)^{0.5}$.

PdAu–ZrO_2-13T sample is higher than the flux for the PdAu–ZrO_2-10T membrane, 1×10^{-1} mol s^{-1} m^{-2} and 0.5×10^{-1} mol s^{-1} m^{-2}, respectively, data taken at 100 kPa. This behavior is in agreement with the higher PdAu film thickness (Fig. 9) of the PdAu–ZrO_2-10T membrane, needed to obtain a dense metallic layer on the support modified with ten deposition-calcination cycles. Additionally, is important to note that the permeation after modification with ZrO_2 did not produce any additional resistance to the overall flux. As shown in Fig. 11, the hydrogen permeation flux for the membranes yielded a linear dependence on the square root of the partial pressure. This trend is consistent with the solution-diffusion mechanism of pure hydrogen through a palladium-alloy membrane, when the rate determining step is the diffusion of H in the metallic alloy bulk film following the Sieverts' Law [24]. The H_2/N_2 ideal selectivity of the studied membranes were 215 and >4000 for the PdAu–ZrO_2-10T and the PdAu–ZrO_2-13T membranes, respectively. A linear dependence has also been reported for PdAg membranes with H_2/N_2 ideal selectivity between 110 and 300 [25]. The flux through the defects and the Sieverts contributions for several PdAg membranes were determined. In all cases the Sieverts contribution was between 97.6 and 99.6% [25].

At 673 K and 100 kPa, the hydrogen flux of the PdAu–ZrO_2-13T membrane was ca. 1×10^{-1} mol s^{-1} m^{-2} (Fig. 11), similar to the hydrogen flux through the PdAu–ZrO_2-5D membranes synthesized on top of ZrO_2 modified porous stainless steel discs with 0.2 μm grade. The selectivity of the PdAu–ZrO_2-13T membrane decreased after three days of evaluations, then the membrane cooled down. This loss of selectivity was attributed to defects at the sealing area formed during the exposure to high temperature, which were detected using a bubble point location test. For that purpose, the membrane was introduced into a vessel with isopropyl alcohol and nitrogen was fed through the membrane. The hydrogen permeabilities of the PdAu–ZrO_2-10T, PdAu–ZrO_2-13T and PdAu–ZrO_2-5D membranes were 9.4×10^{-9} mol s^{-1} m m^{-2} $Pa^{-0.5}$, 9.6×10^{-9} mol s^{-1} m m^{-2} $Pa^{-0.5}$ and 1.0×10^{-8} mol s^{-1} m m^{-2} $Pa^{-0.5}$, respectively. These data are similar to those reported in the literature for PdAu membranes. A hydrogen permeability of ca. 1.36 10^{-8} mol s^{-1} m m^{-2} $Pa^{-0.5}$ at 673 K and differential pressure of 138 kPa has been reported for a 2.3 μm thick $Pd_{95}Au_5$

Please cite this article in press as: Contardi I, et al., Effect of the porous stainless steel substrate shape on the ZrO_2 deposition by vacuum assisted dip-coating, International Journal of Hydrogen Energy (2017), http://dx.doi.org/10.1016/j.ijhydene.2017.01.024

membrane on top of a commercially available YSZ-modified PSS tube [6]. Way and coworkers [26] reported hydrogen permeabilities ranging from 0.7 up to 1.1 10^{-8} mol s^{-1} m m^{-2} $Pa^{-0.5}$ for self-supporting PdAu membranes.

Conclusions

Planar and tubular porous stainless steel substrates were used to obtain ZrO_2 coated porous stainless steel supports for the synthesis of PdAu alloy composite membranes. The vacuum assisted dip-coating process has been optimized on tubular supports by the employment of successive ZrO_2 deposition-calcination cycles.

The H_2/N_2 ideal selectivity values higher than 4000 indicated that dense and continuous palladium-gold layers were deposited on the outer surface of the ZrO_2-modified PSS tube after thirteen ZrO_2 deposition calcination cycles. A complete alloy formation was obtained even after annealing at 723 K at in hydrogen stream during 5 days, as confirmed by cross-section EDS mapping and XRD diffraction analysis.

Even though planar and tubular supports have the same porous grade (0.2 μm) as reported by the manufacturer, the deposition of the ZrO_2 intermetallic layer is not equal in both shapes. This is due to the different support properties at the surface (especially the pore size and defect distribution).

Acknowledgments

The authors wish to acknowledge the financial support received from UNL (CAID 00052LI), ANPCyT (PICT 1948), and CONICET. They are also grateful to Prof. Elsa Grimaldi for the English language editing, to Rubén Mutal for the Confocal Laser Microscopy measurements and to Fabio Fontanarrosa from the CCT CONICET-Santa Fe for the SEM-analyze.

REFERENCES

[1] Iulianelli A, Liguori S, Vita A, Italiano C, Fabiano C, Huang, et al. The oncoming energy vector: hydrogen produced in Pd-composite membrane reactor via bio-ethanol reforming over Ni/CeO_2 catalyst. Catal Today 2016;259:368–75.
[2] Su C, Jin T, Kuraoka K, Matsumura Y, Yazawa T. Thin palladium film supported on SiO_2-Modified porous stainless steel for a high-hydrogen-flux membrane. Ind Eng Chem Res 2005;44:3053–8.
[3] Tonga J, Sua C, Kuraoka K, Suda H, Matsumura Y. Preparation of thin Pd membrane on CeO_2-modified porous metal by a combined method of electroless plating and chemical vapor deposition. J Membr Sci 2006;269:101–8.
[4] Gao H, Li Y, Lin JYS, Zhang B. Characterization of zirconia modified porous stainless steel supports for Pd membranes. J Porous Mater 2006;13:419–26.
[5] Bosko ML, Ojeda F, Lombardo EA, Cornaglia LM. NaA zeolite as an effective diffusion barrier in composite Pd/PSS membranes. J Membr Sci 2009;331:57–67.
[6] Hatlevik Ø, Gade SK, Keeling MK, Thoen PM, Davidson AP, Way JD. Palladium and palladium alloy membranes for hydrogen separation and production: history, fabrication strategies, and current performance. Sep Purif Technol 2010;73:59–64.
[7] Lundin STB, Law JO, Patki NS, Wolden CA, Way JD. Glass frit sealing method for macroscopic defects in Pd-based composite membranes with application in catalytic membrane reactors. Sep Purif Technol 2017;172:68–75.
[8] Sanz R, Calles JA, Alique D, Furones L, Ordóñez S, Marín P, et al. Preparation, testing and modelling of a hydrogen selective Pd/YSZ/SS composite membrane. Int J Hydrogen Energy 2011;36:15783–93.
[9] Tarditi AM, Gerboni C, Cornaglia L. PdAu membranes supported on top of vacuum-assisted ZrO_2-modified porous stainless steel substrates. J Membr Sci 2013;428:1–10.
[10] Zhang K, Gao H, Rui Z, Liu P, Li Y, Lin YS. High-temperature stability of palladium membranes on porous metal supports with different intermediate layers. Ind Eng Chem Res 2009;48:1880.
[11] Okazaki J, Ikeda T, Pacheco Tanaka DA, Llosa Tanco M, Wakui Y, Sato K, et al. Importance of the support material in thin palladium composite membranes for steady hydrogen permeation at elevated temperatures. Phys Chem Chem Phys 2009;11:8632–8.
[12] Ayturk ME, Ma YH. Electroless Pd and Ag deposition kinetics of the composite Pd and Pd/Ag membranes synthesized from agitated plating baths. J Membr Sci 2009;330:233–45.
[13] Yuna S, Oyama ST. Correlations in palladium membranes for hydrogen separation: a review. J Membr Sci 2011;375:28–45.
[14] Gallucci F, Fernandez E, Corengia P, Annaland M. Recent advances on membranes and membrane reactors for hydrogen production. Chem Eng Sci 2013;92:40–9.
[15] Ayturk ME, Engwall EE, Ma YH. Microstructure analysis of the intermetallic diffusion-induced alloy phases in composite Pd/Ag/porous stainless steel membranes. Ind Eng Chem Res 2007;46:4295–306.
[16] Yepes D, Cornaglia LM, Irusta S, Lombardo EA. Different oxides uses as diffusion barriers in composite hydrogen permeable membranes. J Membr Sci 2006;274:92–101.
[17] Bonekamp BC. In: Burggraaf AJ, Cot L, editors. Preparation of asymmetric ceramic membrane supports by dip-coating in fundamentals of inorganic membrane science and technology. Amsterdam: Elsevier; 1996.
[18] Mardilovich IP, Engwall E, Ma YH. Dependence of hydrogen flux on the pore size and plating surface topology of asymmetric Pd-porous stainless steel membranes. Desalination 2002;144:85–9.
[19] Chi YH, Hsu W-F, Huang T-Q, Yang Ch, Lin Y, Jeng M. Thin Pd membrane on a modified porous stainless steel tube: Al_2O_3 particle size selection strategy. J Chin Inst Eng 2011;34:49–55.
[20] Huang Y, Dittmeyer R. Preparation and characterization of composite palladium membranes on sinter-metal supports with a ceramic barrier against Intermetallic diffusion. J Membr Sci 2006;282:296–310.
[21] Calles JA, Sanz R, Alique D, Furones L. Thermal stability and effect of typical water gas shift reactant composition on H_2 permeability through a Pd-YSZ-PSS composite membrane. Int J Hydrogen Energy 2014;39:1398–409.
[22] Shi L, Goldbach A, Zeng G, Xu H. Preparation and performance of thin-layered PdAu/ceramic composite membranes. Int J Hydrogen Energy 2010;35:4201–8.
[23] Shi L, Goldbach A, Xu H. High-flux H_2 separation membranes from (Pd/Au)n nanolayers. Int J Hydrogen Energy 2011;36:2281–4.
[24] Al Mufachi NA, Rees NV, Steinberger-Wilkens R. Hydrogen selective membranes: a review of palladium-based dense metal membranes. Ren Sust Energy Rev 2015;47:540–51.

Please cite this article in press as: Contardi I, et al., Effect of the porous stainless steel substrate shape on the ZrO_2 deposition by vacuum assisted dip-coating, International Journal of Hydrogen Energy (2017), http://dx.doi.org/10.1016/j.ijhydene.2017.01.024

[25] Bosko ML, Lombardo EA, Cornaglia LM. The effect of electroless plating time on the morphology, alloy formation and H_2 transport properties of PdAg composite membranes. Int J Hydrogen Energy 2011;36:4068–78.

[26] Gade SK, Payzant E, Park J, Thoen PM, Way JD. The effects of fabrication and annealing on the structure and hydrogen permeation of Pd–Au binary alloy membranes. J Membr Sci 2009;340:227–33.

Please cite this article in press as: Contardi I, et al., Effect of the porous stainless steel substrate shape on the ZrO_2 deposition by vacuum assisted dip-coating, International Journal of Hydrogen Energy (2017), http://dx.doi.org/10.1016/j.ijhydene.2017.01.024